scientific reports

Check for updates

OPEN

A new type of aircraft icing detection system

Nilton O. Renno[1,2]✉, Roger Backhus[3,4], Timothy Butler[3,4], Curt Cooper[2,3,4], Kurt A. Hochrein[2,4], Rohan Madathil[1], Louis Marr[3,4], Ryan Miller[2,3,4], Paul Mohan[2,4], Stephen Musko[2,4], Thomas Ryan[2,4], Fernando Saca[3,4] & Jeffrey Zewicke[2,4]

Ice accretion by the impact of supercooled water drops, or mixtures of these drops with ice, onto an aircraft in flight is a hazard referred to as icing. Aircraft certified to fly in icing conditions like airliners, currently have simplistic icing detection probes. Aircraft certification specifications recently developed in response to the discovery that ice accretion by the impact of supercooled large droplets (SLDs) has caused many aircraft accidents imply the need for an icing detection system (IDS) capable of discerning between ordinary icing conditions and the more hazardous SLD icing conditions. It is desirable that these new IDS be capable of measuring both the ice accretion onto the aircraft and the icing-hazard potential of the atmosphere around the aircraft. We report the development and flight test of an IDS consisting of a microwave resonator unit to measure ice accretion onto the aircraft and an optical unit to estimate the icing-hazard potential of the atmosphere around the aircraft. The results of flight tests in a jet aircraft with reference scientific measurements indicate that our new IDS is capable of detecting ice accretion in the aircraft and of discriminating between common icing conditions and the more hazardous SLD icing conditions.

Keywords Aircraft, Ice, Icing, SLD, Safety

Icing can be a hazard for aircraft that fly in ubiquitous water or mixed phase clouds at temperatures below 0° C[1,2]. There is evidence that about 10% of all fatal air carrier accidents have been caused by icing[3], and that icing was responsible for some of the most catastrophic aircraft accidents of the past few decades because it can cause loss of control[4]. Recently, modern commercial transport aircraft have suffered catastrophic icing-related accidents[5]. For example, the August 2024 Voepass ATR 72-500 crash in Brazil that killed 62 people appears to have been triggered by ice accretion onto the aircraft[6]. Therefore, detecting the potential for icing hazards in enough time for the aircraft to activate its ice protection system before significant ice accretion occurs, increase power, and escape icing conditions is extremely important for aviation safety.

In the United States, the Federal Aviation Administration (FAA) requires manufacturers to demonstrate that newly designed aircraft are capable of flying safely under icing conditions specified in the Federal Airworthiness Regulations (FAR). FAA certification procedures are updated regularly as a result of lessons learned during accident investigations[7]. Since 1994 the FAA has issued hundreds of Airworthiness Directives (AD) to address icing safety on more than 50 types of aircraft[8]. These airworthiness directives cover safety issues ranging from crew operating procedures in icing conditions to aircraft design changes. The Federal Aviation Administration (FAA) also requests changes to aircraft flight manuals (AFM) and other aircraft operations documents to address icing problems.

Aircraft certification standards define environment conditions conducive to icing, such as cloud liquid water content (*LWC*), supercooled liquid water drop size (specified either as drop mean effective diameter *MED* or drop median volume diameter *MVD*), air temperature and altitude ranges in which manufacturers must show that their newly designed aircraft can fly safely in. These conditions are referred to as flight certification envelopes. The icing flight certification envelopes of the classic Aircraft Certification Specifications (ACS) procedures that have been in effect since 1964 are referred to as Appendix C icing conditions, while the icing conditions recently added to the ACS that include the less common but more hazardous Supercooled Large Droplet (SLD), including freezing drizzle (FZDZ) and freezing rain (FZRA) are referred to as Appendix O icing conditions.

Aircraft certified to fly under icing conditions are required to go through extensive verification procedures intended to ensure they can operate safely under the icing certification conditions specified in the regulations,

[1]Department of Climate and Space Sciences and Engineering, University of Michigan, Ann Arbor, MI 48109, USA. [2]Intelligent Vision Systems, Dexter, MI 48130, USA. [3]Space Physics Research Laboratory, University of Michigan, Ann Arbor, MI 48109, USA. [4]Roger Backhus, Timothy Butler, Curt Cooper, Kurt A. Hochrein, Louis Marr, Ryan Miller, Paul Mohan, Stephen Musko, Thomas Ryan, Fernando Saca and Jeffrey Zewicke contributed equally to this work. ✉email: renno@alum.mit.edu

for example in the United States by 14 Code of Federal Regulations (CFR) Part 25 and in Europe by Certification Specifications (CS) 25, for transport category airplanes[9]. This certification process typically includes extensive icing safety verification procedures using computer models, wind tunnel tests, clear-air tests, tests behind icing tankers, and flight in natural icing conditions. The objective of these certification procedures is to verify that the aircraft being certified has an adequate icing protection system and acceptable performance and flight handling qualities while escaping hazardous icing conditions. A reliable icing detection system capable of discerning Appendix C from the more hazardous Appendix O icing conditions not only increases flight safety by quickly alerting the flight crew to potential problems, but also by reducing the time period from detection to exiting the icing conditions. This is important because manufacturers must demonstrate that the aircraft being certified is capable of flying safely even under the most hazardous icing conditions while exiting these potentially catastrophic icing conditions.

The definition of Appendix C icing conditions is divided into continuous conditions found in stratiform clouds defined as on average 17.4 nautical miles long, with relatively low water content, reaching altitudes of up to 22,000 feet and temperature as low as -30° C, and in intermittent conditions found in cumuliform clouds defined as on average 2.6 nautical miles long, with higher water content, reaching altitudes of up to 30,000 feet and temperature as low as -40° C. In intermittent conditions, the maximum drop mean effective diameter (*MED*) specified in Appendix C conditions is 50 μm, for cloud liquid water content above the measurable minimum (in practice, independently of the cloud liquid water content). In continuous conditions, the maximum drop mean effective diameter (*MED*) is 40 μm, for cloud liquid water content above the measurable minimum[9]. In these conditions, drop mean effective diameter (*MED*), and drop median volume diameter (*MVD*) are in practice undistinguishable from each other. The definition of Appendix O icing conditions is split into two parts. Part I defines the Appendix O meteorology. It defines freezing drizzle (FZDZ) as conditions with spectra maximum drop diameter between $100\,\mu\text{m}$ and $500\,\mu\text{m}$, freezing rain (FZRA) as conditions with spectra maximum drop diameter larger than $500\,\mu\text{m}$; it also defines the liquid water content, drop size distribution, and horizontal extent of these conditions. Overall, Part I defines Appendix O conditions as those with supercooled large drops (SLDs) in which drop median volume diameter (*MVD*) is either smaller than $40\,\mu\text{m}$ (and the liquid water content is higher) or larger than $40\,\mu\text{m}$ (and the liquid water content is lower), the maximum mean effective drop diameter (*MED*) of Appendix C continuous maximum (stratiform clouds) icing conditions. In Appendix O, supercooled large drop (SLD) icing conditions consist of freezing drizzle and freezing rain that occur in and/or below stratiform clouds, with maximum diameter larger than $100\,\mu\text{m}$. Part II defines ice accretions that shall be used to show compliance with the requirements for airplane performance and handling qualities[10,11].

The detailed specification of Appendix O icing conditions is necessary for manufacturers to determine the ice accretions that shall be used to show compliance with the requirements for airplane performance and handling qualities. Since it follows from the definition of Appendix C conditions that when the drop mean effective diameter (*MED*) is larger than $40\,\mu\text{m}$, the airplane is in more hazardous conditions than those of Appendix C, it implies that in this case the airplane is in Appendix O icing conditions. Thus, conservatively we can state that whenever an airplane encounters drop of median volume diameter larger than about $40\,\mu\text{m}$ (in practice, $MVD \simeq MED$) it is in Appendix O icing conditions, if these conditions persist for more than the few minutes necessary for the airplane to cover the specified distance (17.4 nautical miles adjusted based on the liquid water content, temperature, and drop spectrum encountered).

None of the icing detection systems currently in use is capable of measuring cloud droplet size or cloud water content; they simply estimate ice accretion onto the aircraft. In addition, current aircraft icing detection systems are based on measurements made by ice accretion probes[12,13] placed away from areas where ice accretion could pose a risk. Ice accretion probes do not detect ice accretion directly where it could create a hazard, such as in wings, horizontal stabilizers, and around flight control surfaces. Dynamic compression of airflow over ice accretion probes, together with the release of latent heat when water freezes, increases the probe temperature and therefore reduces its collection efficiency in the most hazardous icing conditions because in them the air temperature is typically close to 0° C[14–16]. However, to mitigate this detection problem, the probes of the most widely adopted ice detection systems contain features that facilitate ice accretion on them at a higher rate than in other parts of the airplane. Fortunately, this is not a problem for flush-mounted sensors that detect ice accretion directly, where it can create a hazard.

Here we describe a new type of aircraft icing detection system (IDS) consisting of a flush mounted microwave resonator unit (MRU) to measure ice accretion anywhere in an aircraft and an optical icing detection unit (OIDU) to measure the icing conditions of the atmosphere around the aircraft. The MRU uses changes in the frequency and the quality factor of one of the resonance modes of a microstrip sensor to detect ice accretion onto the aircraft[17], while the OIDU uses reflectance signals in three short-wave infrared (SWIR) bands to estimate the thermodynamic phase of cloud water, the size of cloud droplets, and the total water content[17–19]. The main advantage of our new aircraft icing detection system is that it detects ice accretion on the aircraft and the icing potential of the atmosphere around the aircraft. Its main disadvantage is that it is more complex than existing systems, including some of the other systems tested in the same flight campaign. Ice accretion affects aircraft performance, handling qualities, and therefore flight safety. In fact, severe ice accretion can cause aircraft loss of control. Together, OIDU and MRU measurements have the potential to meet all requirements of the revised regulations specified in European Organisation for Civil Aviation Equipment (EUROCAE) ED-103B, also published as SAE AS5498[10,11], but, as discussed below, measurements under real-world conditions pose multiple challenges to these technologies. We show that the IDS overcomes most of these challenges and is capable of not only detecting when the aircraft encounters icing conditions but also distinguishing the common Appendix C icing conditions from the more hazardous Appendix O icing conditions.

Recent developments

Recent changes in aircraft certification specifications (ACS) motivated the development of new icing detection technologies. To our knowledge, this was pioneered by United Technologies Corporation (UTC) in developing an optical icing detection (OID) system[20,21] that uses polarimetry to determine the thermodynamic phase of cloud water[22] and backscatter to determine the size and water content of cloud drops.[20] UTC's OID has similarities with our own optical icing detection unit (OIDU), but it samples a orders of magnitude smaller atmospheric volume and is more complex because it requires the polarization of the light it emits and measurements of the depolarization of the backscattered light received, instead of requiring simpler measurements of ratios of backscattering signals. Light depolarization is caused not only by ice particles but also by multiple scattering in water drops, making its use for thermodynamic phase detection unreliable when the cloud liquid water content is high. Moreover, mixed thermodynamic phase conditions also depolarize the light signal, further complicating thermodynamic phase detection. The OIDU is simpler and produces more reliable results because light absorption and backscattering in the three narrow bands selected depend primarily only on the thermodynamic phase of the cloud water, the cloud drop size, and the cloud water content. Moreover, multiple scattering enhances the thermodynamic phase detection by the OIDU method, rather than degrading the detection.

The changes in Aircraft Certification Specifications (ACS) inspired the establishment of the European Union (EU)-funded SENSors and certifiable hybrid architectures for safer aviation in ICing Environment (SENS4ICE) consortium, to address the need for more reliable icing detection systems capable of discriminating between Appendix C and Appendix O conditions[23]. One of the main goals of the SENS4ICE consortium was to mature and test new technologies that have the potential to meet the requirements imposed by the new ACS[10,11]. In fact, the SENS4ICE consortium supported the development and testing of ten new aircraft icing detection technologies, including a novel detection approach which combines direct detection of atmospheric icing conditions and ice accretion onto the aircraft, with indirect detection of icing by monitoring changes in aircraft flight characteristics caused by ice accretion[24].

The icing detection technologies whose developments were supported by the SENS4ICE consortium are described in Deiler (2024)[24]. They consist of the detection of icing conditions by: (1) Measuring changes in heat flux icing causes on surface-mounted heated probes like AeroTex's Atmospheric Icing Patch (AIP)[25], and Collins Aerospace's Icing Detection System (Collins' IDS)[26]; (2) Measuring the characteristics of ultrasonic waves propagating in the aircraft's surface that depend on the amount of ice accreted like DLR's Local Ice Layer Detector (LILD)[27]; (3) Measuring temperature variations caused by ice accretion like INTA's Fiber Optic Detector (FOD)[28,29]; (4) Measuring hydrometeors size distribution based on particle scattering like Honeywell's Short-Range Particulate (SRP)[23]; (5) Estimating hydrometeors' size by measuring their charging by corona discharge like ONERA's Atmospheric Hydrometeor Detector based on Electrostatics (AHDEL)[23]; (6) Measuring charge accumulation on an aircraft by a network of electric field mills to estimate the cloud total water content like ONERA's Atmospheric Measurement of Potential and ElectRic field on Aircraft (AMPERA)[23]; (7) Imaging hydrometeors to estimate their size and total water content like SAFRAN's Appendix O Discriminator (AOD)[23]; and (8) Estimating atmospheric icing conditions by measuring ice accretion rate on a compact ice catch probe like SAFRAN's Primary in-Flight Icing Detection System (PFIDS)[23].

The developments of ONERA's Atmospheric Hydrometeor Detector based on Electrostatics (AHDEL) and SAFRAN's Appendix O Discriminator (AOD) were discontinued prior to the SENS4ICE flight campaigns due to unsatisfactory performance in tests prior to the flight campaigns[24]. Eight direct icing detection technologies, including our own icing detection system (IDS), were tested in SENS4ICE flight campaigns, together with the complementary hybrid approach[24]. Analysis of flight test data reported by Deiler (2024)[24] indicates that Honeywell's Short-Range Particulate (SRP) was unable to detect the less severe Appendix C icing conditions, INTA's Fiber Optic Detector (FOD) measurements were noisy because changes in both temperature and cloud water content affect its signal, and SAFRAN's Primary in-Flight Icing Detection System (PFIDS) was unable to discriminate between Appendices C and O icing conditions. ONERA's Atmospheric Measurement of Potential and ElectRic field on Aircraft (AMPERA) primary goal was the detection of charging caused by the impact of hydrometeors onto the aircraft, not icing; it was developed primarily for the detection of volcanic ash. The best performing SENS4ICE technologies appear to have been Collins Aerospace's IDS and AeroTex's Atmospheric Icing Patch (AIP)[24], but the response of AIP to icing conditions degraded during the test flight campaign[24]. Of all the sensors tested, only Collins Aerospace's Icing Detection System (Collin's IDS)[24] and our own icing detection system (IDS) appear to have been able to discern the icing conditions of Appendix C from those of Appendix O throughout the flight tests. In addition, INTA's Fiber Optic Detector (FOD) has been reported to be able to discern between Appendix C and Appendix O icing conditions when the cloud liquid water content was high[29]. Collins Aerospace's IDS correlates measurements of the heat flux in a portion of the aircraft with atmospheric icing conditions, while INTA's FOD correlates measurements of variations in the temperature along a fiber optic with icing atmospheric conditions; they do not measure the icing potential of the atmosphere around the aircraft directly like our technology does.

The Phenom 300 jet used a Science Engineering Associates Ice Crystal Detector (ICD) for reference scientific measurements of total water content (*TWC*), liquid water content (*LWC*), and ice water content (*IWC*). The ICD measurement errors are estimated to be about ±10% for *LWC*, about ±40% for *IWC* in glaciated conditions. A Droplet Measurement Technologies single particle light scattering cloud droplet probe (CDP) was used to measure droplet size from 2 to 50 μm and their *LWC* based on scattering in the forward direction. The accuracy of the CDP estimation of drop *MVD* is about ±20%. The accuracy of the CDP *LWC* measurements in non-precipitating clouds is about 10-15%, and of *LWC* in precipitation is about ±40%. A Droplet Measurement Technologies single particle cloud imaging probe (CIP) was used to measure the size of particles of diameters ranging from 25 to 1,550 μm. The CIP estimates hydrometeors size and shape based on 2-dimensional imaging. The accuracy of CIP MVD estimates is about ±20%. The accuracy of the CIP *LWC* estimates is about ±40%[24]. In

summary, the errors in the measurements of *MVD* are about ±20%, and in the measurements of *TWC* they are about ± 40%.

As discussed in this article, sampling volume and location mismatches, the limited range of conditions encountered during the flight campaign, and the large measurement errors prevented a complete assessment of the performance of our new aircraft icing detection system (IDS). Here we describe the general features of the IDS and discuss the results of its flight tests on Embraer's Phenom 300 jet aircraft containing reference scientific instruments to assess the quality of measurements with icing detection systems[24]. The flight tests were part of the SENSE4ICE campaign in which we participated as Embraer's collaborator, not as member of the SENSE4ICE consortium.

Our new aircraft icing detection system (IDS)

Our Icing Detection System (IDS) was designed to be an active in-flight icing detection system (FIDS) capable of meeting the ED-103B requirements[11]. Moreover, the IDS was designed to meet the Minimum Operational Performance Specification (MOPS) for Active on-board In-Flight Ice Detection Systems (AFIDS) by detecting ice accretion onto the aircraft, detecting conditions conducive to icing in the atmosphere around the aircraft, and discriminating between Appendix C and Appendix O icing conditions in the atmosphere around the aircraft. The IDS was also designed to comply with the Radio Technical Commission Environmental Conditions and Test Procedures for Airborne Equipment standard (DO-160)[30] for environmental tests of avionic hardware.

The IDS Microwave Resonator Unit (MRU) was designed not only to detect ice accretion onto aircraft surfaces but also to determine if this ice is pure like rime ice or if it is mixed with water like glaze ice, and then estimate the ice thickness. In addition, the MRU was designed to measure the thickness of liquid-water films on the aircraft surface to infer cloud liquid water content (LWC). Microwave resonators were originally developed to measure soil dielectric properties and water content of snow and soils[31–33], but have also been used to characterize the complex permittivity of industrial materials[34,35].

The primary function of the MRU is to inform the flight crew or aircraft systems about possible degradation of flight performance by ice accretion onto aircraft surfaces. MRU sensors are designed to be flush mounted on the surfaces of interest, and each MRU sensing unit has a heater that can be used to control ice accumulation. This allows the melting of ice accreted on the microstrip resonator to measure the ice accumulation rate or the thickness of water films if the heater is kept on. Multiple MRU sensors can be installed on the aircraft, for example, to detect ice accretion in protected areas, runback ices directly where they could cause control problems, or to measure water film thickness directly on heated surfaces to estimate cloud liquid water content.

The primary function of the IDS optical icing detection unit (OIDU) is to interrogate the atmosphere around the aircraft to determine whether it contains supercooled liquid water, a mixed thermodynamic phase (mixtures of ice and water), ice or is clear. If liquid water or mixed phase are detected, the OIDU determines if the aircraft is flying under icing conditions of Appendix C or Appendix O, estimates the median volume diameter (*MVD*) of the cloud drops, and estimates the total water content (*TWC*) of the cloud. The OIDU then reports the absence or presence of conditions conducive to icing in the atmosphere around the aircraft, whether the aircraft is flying under Appendix C or Appendix O conditions, and the hazard level based on the estimated values of *MVD* and *TWC*. Some technical details on the IDS, including specific design features and results of laboratory and ground tests with prototypes and the flight unit, are provided in the supplementary information.

The use of a technology to measure ice accretion onto the aircraft and a completely different technology to determine the icing-hazard potential of the atmosphere around the aircraft makes the IDS a robust instrument with the potential to contribute significantly to flight safety.

The microwave resonator unit (MRU)

The MRU is based on the principle that the center frequency (f_i) and the quality factor ($Q_i \equiv \frac{f_i}{\Delta_{f_i}}$) of the resonance modes $i = 1, 2, 3..., n$ (where n is an integer) of a microstrip sensor are a function of the complex permittivity of the substance in contact with it, where Δ_{f_i} is the half-power bandwidth of the resonance mode i [18,33,36]. The frequency f_i of the resonance mode i depends on the speed of the electromagnetic wave propagating on the microstrip, which in turn depends on the real part of the complex permittivity of the substance in contact with it. When the MRU's microstrip resonator is dry, this substance is air. In the frequency range that covers the peak power of the fundamental mode ($f_1 \approx 0.9$ GHz) and the entire first three harmonics (in the range $0.5 - 3.5$ GHz as shown in the supplementary information) of the microstrip resonances, the real part of the complex permittivity of ice is about 30 times higher than that of air[37]. This causes even submillimeter layers of ice to shift the microstrip resonance frequency significantly. The quality factor (Q_i) of the resonance mode i depends on the damping of electromagnetic waves propagating in the microstrip, which in turn depends on the imaginary part of the permittivity of the substance in contact with the microstrip[38]. The imaginary part of the permittivity of water is about 10^4 larger than that of ice in the $0.5 - 3.5$ GHz frequency range, and is even higher for deicing fluid. Thus, Q_i can be used to distinguish even submillimeter thick layers of these substances from each other[36].

The MRU electronics are capable of measuring the frequencies (f_i) and quality factors (Q_i) of the first three modes ($i = 1, 2, 3$) of the resonances of the microstrip. The third mode with a peak power at a frequency of about 2.65 GHz, with the microstrip dry, is selected for the MRU measurements because this mode is the most sensitive to the substances of interest, as shown in the supplementary information. The MRU radio frequency (RF) circuit measures the resonance power as a function of frequency based on the microwave signal transmitted from port 1 and received at port 2, that is the ($|S_{21}|^2$) scatter parameter[38]. The MRU is calibrated by measuring the resonance frequency and quality factor with the microstrip resonator dry (unloaded) and loaded with layers of substances of interest of various thicknesses. Then a lookup table is developed to fingerprint the substances

of interest and quantify the amount deposited on the microstrip as discussed in the literature[33]. Petersan and Anlage (1998)[39] discuss a more sophisticated method to estimate the permittivity of substances in contact with microstrip resonators, but the results of our numerical simulations and laboratory tests indicate that this more complex approach is not necessary for the detection of ice accretion.

A microcontroller controls the MRU and processes the data from measurements between about 2.0 and 3.0 GHz to determine the center frequency f_3 and the quality factor Q_3. The MRU electronics contain an oscillator and a synthesizer to generate an RF signal, an attenuator to mitigate reflections from the microstrip resonator, a power detector, an amplifier, a low-pass filter, and an analog-to-digital converter to convert the analog signal to digital before it is sent to the microcontroller for analysis. In addition, the MRU contains digital-to-analog converters, a power supply, heaters, temperature sensors, and health monitoring sensors. A switch is added to the prototype to provide access to external signal generators during tests and calibrations. The complete MRU consists of a main electronics board, an RF board, at least one microstrip resonator, and an auxiliary sensor board containing heaters and temperature sensors.

The optical icing detection unit (OIDU)

The OIDU is an atypical three-band lidar capable of measuring the thermodynamic phase of cloud water, the size of cloud drops, and the total water content. Its optical subsystem consists of three lasers to illuminate the cloud, illumination optics to combine the three laser beams into a single output beam, which is coaxial and co-divergent with the receiver field of view, to ensure that the cloud volume illuminated and the cloud volume viewed by the OIDU are the same at any distance probed, and receiver optics. The illumination and receiver paths are optically isolated from each other to optimize the measurement signal-to-noise ratio. The OIDU emits time-sequenced laser pulse trains centered on wavelengths λ_1, λ_2, and λ_3, with adjustable individual pulse duration set to 50 ns in the flight unit. The backscatter signals from each laser pulse train received by the OIDU are processed by a field-programmable gate array (FPGA) to produce statistics like the mean background and backscatter signals in each measurement wavelength λ_j, where $j = 1, 2, 3$. The distance from the instrument window to the portion of the cloud that is illuminated by the laser-pulse trains and analyzed, and the cloud volume illuminated during the measurements, can be controlled to optimize the backscatter signal (see supplementary information). In the flight unit, the cloud measurements are set to begin at 50 m from the instrument window and cover a cloud volume of approximately 8.3 m^3. The laser firing and receiver timings can be dynamically adjusted to optimize the signals under different atmospheric conditions, but they were fixed during the flight test.

The OIDU measurement technique is derived from remote sensing methods developed to estimate the thermodynamic phase of cloud particles, the liquid water path and the size of cloud drops[40–48] and a lidar measurement method developed to estimate the size of the drops and the liquid water content of the drizzle[49]. Narrowband (10-nm) measurements centered on wavelengths $\lambda_1 = 1635$ nm and $\lambda_2 = 1525$ nm were selected to determine the thermodynamic phase of cloud particles because the absorption coefficient (the imaginary part of the refractive index) for ice differs significantly from that of liquid water in these two bands[48], and the relative effect of the size of the cloud drop on the backscatter signal is insignificant[41]. Narrowband (5-nm) measurements centered at $\lambda_3 = 905$ nm were selected because the absorption coefficient for liquid water and ice is about 3 orders of magnitude smaller in this wavelength than at 1525 and 1635 nm[50], and together with measurements at one of the longer wavelengths, the cloud drop size and total water content can be inferred from them. In fact, Westbrook et al.[49] show that by selecting one laser at a weakly absorbing wavelength like $\lambda_3 = 905$ nm and the other near the peak absorption by water drops like $\lambda_2 = 1525$ nm, the ratio of the backscatter signal at these wavelengths in drizzle depends on *MVD*, while the backscatter signal at $\lambda_3 = 905$ nm depends on the liquid water content.

The power of the return signal $P_{\lambda_j}(z)$ from the laser of wavelength λ_j illuminating the cloud at distance z is

$$P_{\lambda_j}(z) = G(z)\sigma_{\lambda_j} P_{\lambda_j}(\theta) e^{-2\alpha_{\lambda_j} z}, \tag{1}$$

where $G(z)$ is the instrument (OIDU) gain or light collection efficiency, σ_{λ_j} is the cloud scattering coefficient at wavelength λ_j, $P_{\lambda_j}(\theta)$ is the scattering phase function at angle θ, and α_{λ_j} is the extinction coefficient at wavelength λ_j.

First, the OIDU determines when the aircraft enters potential icing conditions and then estimates the thermodynamic phase of the cloud particles by calculating the ratio of the lidar backscatter signals at wavelength $\lambda_2 = 1525$ nm with those at wavelength $\lambda_1 = 1635$ nm, that is

$$\gamma = \frac{P_{\lambda_2}(z)}{P_{\lambda_1}(z)}, \tag{2}$$

where as shown in the supplementary information the calibration of the OIDU indicates that outside clouds and for ice particles $\gamma < 0.76$, for liquid water phase $\gamma > 0.82$, and for mixed thermodynamic phase γ is between these two values. If liquid water or mixed thermodynamic phase is detected and the outside air temperature is below a predetermined threshold value such as 0° C, the OIDU determines whether the aircraft is flying under Appendix C or Appendix O icing conditions. The air temperature during the Phenom 300 flights in icing conditions was typically between -10 and -5° C. As indicated in the Supplementary Information, OIDU measurements are sensitive to the internal temperature of the OIDU, but since the internal temperature sensor was not active in the unit used in the flight campaign and this sensitivity is small between −10 and −5° C, temperature corrections were not applied to any of the OIDU measurements reported in this article. We plan to install a heater to control the internal temperature of the OIDU before future flight tests and we already activated the OIDU internal temperature sensor.

The top-level requirement of the OIDU is to discriminate between the icing conditions of Appendix C and Appendix O. A cloud with a median volume diameter (*MVD*) greater than 40 μm implies Appendix O conditions at any liquid water content (*LWC*) simply because it implies SLD conditions. Since for drops with *MVD* larger than about 40 μm the extinction coefficient is approximately independent of wavelength λ_j of the lidar signal[49], it follows from eqn (1) that the ratio of the signal from laser λ_3 to that of laser λ_2, that is

$$\alpha \equiv \frac{P_{\lambda_3}(z)}{P_{\lambda_2}(z)} \approx \frac{\sigma_{\lambda_3} P_{\lambda_3}(\theta)}{\sigma_{\lambda_2} P_{\lambda_2}(\theta)} \propto \frac{a}{f(MVD)}, \tag{3}$$

where *a* and is a constant and *f*(*MVD*), is a polynomial function. Thus, the parameter α can be used to discern Appendix C from Appendix O icing conditions. The inverse relationship between α and *f*(*MVD*) is due to the fact that the OIDU detector is time-gated to start recording return signals only after each complete laser pulse train reaches a distance of 50 m in the cloud and the scattering signals received are those traveling back to the OIDU (for a round-trip distance of 100 m), implying that physically when viewed from where the laser pulse is illuminating the cloud, the dominant scattering angle is $\theta = 0^\circ$, instead of 180° as in typical lidars that primarily measure the scattering of the outgoing signal (see illustration in the supplementary information). Thus, the OIDU is an atypical lidar because measurements are made with the aircraft immersed in clouds or precipitation, and while the received signals are being recorded, the laser pulse is illuminating the cloud or precipitation along scattered laser light paths pointing towards the aircraft, from a cloud volume more than 50 m away from the OIDU.

The Phenom 300 reference scientific instruments measured cloud properties (e.g. *MVD*, *LWC*, *TWC*) in a small sampling volume (of the order of cm^3) next to the airplane[24], while the OIDU measured cloud properties at 50 m from the airplane towards its left side, and on a volume of approximately 8.3 m^3 as indicated in the supplementary information. To mitigate this sampling mismatch, we compare mean values of the quantities of interest in 120 s measurement intervals. The mean values of these quantities for each flight segment in icing conditions are presented in Table 1. Data points reported to contain measurement errors (identified by the NAN code in the data) and in-cloud measurements in which $TWC \leq 0$ or $MVD \leq 0$ were removed prior to analysis. Using Phenom 300 data from all flight campaign segments[51], summarized in Table 1, in which $TWC \geq 0.2$ g/m^3 (the water content on the low *MVD* edge of the icing envelope of Appendix C) to calibrate OIDU measurements, we find $MVD = \frac{1.740}{\alpha - 0.289}$ and $\hat{TWC} = 0.354e^{-0.004MVD}$ where $\alpha \geq 0.2925$, as shown in Fig.1 a and b. The units of the parameters used in these two equations are those specified in Table 1. It is well known that in a specific cloud, cloud drop size varies less than cloud drop number density and therefore water content (see Fig. 3 of Renno et al. (2013) for an example)[47]. Thus, sampling errors due to the mismatches

Flight #	Time int (s)	Appendix	MVD (μm)	LWC (g/m^3)	TWC (g/m^3)	α	β	γ
1475 - Int 1	63739 - 64368	C	17	0.56	0.64	0.38	1.65	0.81
1475 - Int 2	64870 - 65295	C	15	0.67	0.76	0.41	1.52	0.79
1477 - Int 1	45372 - 45532	O	59	0.59	0.79	0.32	1.53	0.82
1477 - Int 2	45896 - 46156	C	26	0.33	0.41	0.33	1.55	0.82
1477 - Int 3	46417 - 46727	C	25	0.30	0.33	0.33	1.75	0.84
1477 - Int 4	47154 - 47306	C	17	0.66	0.78	0.38	2.01	0.84
1477 - Int 5	47678 - 48058	C	38	0.30	0.35	0.33	1.58	0.82
1477 - Int 6	48550 - 48728	C	12	0.11	0.12	0.31	1.35	0.81
1477 - Int 7	48978 - 49217	C	21	0.30	0.34	0.34	1.56	0.82
1479 - Int 1	43667 - 43773	O	87	0.18	0.23	0.32	1.49	0.82
1479 - Int 2	46786 - 47247	O	163	0.22	0.24	0.30	1.18	0.79
1479 - Int 3	47452 - 47716	O	61	0.09	0.11	0.30	1.03	0.77
1481 - Int 1	45625 - 45678	C	17	0.15	0.17	0.33	1.19	0.78
1481 - Int 2	45713 - 46197	C	21	0.42	0.48	0.36	1.52	0.81
1482 - Int 1	60712 - 61240	C	15	0.49	0.51	0.36	–	1.03
1482 - Int 2	61420 - 61913	C	14	0.49	0.50	0.36	–	1.02

Table 1. Summary of the Phenom 300 data for flight intervals (Int) in which the IDS was turned on. The flight numbers, the flight time intervals in seconds of the day in Greenwich (UTC), and the determination of whether the flight interval was in Appendix C or Appendix O icing conditions are from the SENS4ICE flight reports[24,51]. The *MVD*, *LWC*, *TWC*, α, β, and γ values are mean values for the time the aircraft was inside cloud, defined as data points in which $MVD > 0$, and $TWC > 0$. Inconsistencies in the reference flight data were mitigated by setting $MVD = 0$ whenever $TWC \leq 0$ or $MVD < 0$. The OIDU temperature was much lower in flight 1482 than in the other flights, and this caused drifts in its measurements making them unreliable, particularly β. As indicated in the supplementary information, γ increases as the OIDU temperature decreases.

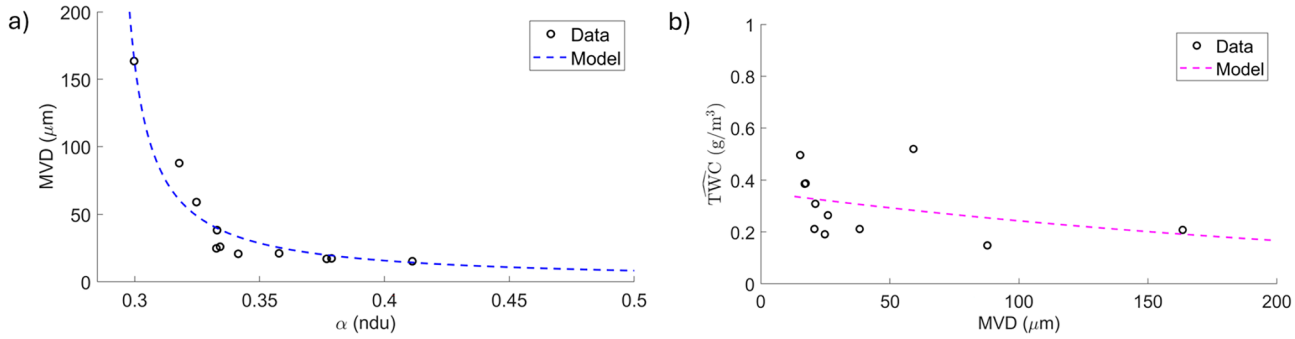

Fig. 1. (**a**) The flight data indicates that 120 s mean values of the cloud drop median volume diameter (*MVD*) is inversely related to 120 s mean values of the parameter $\alpha \equiv \frac{P_{\lambda_3}(z)}{P_{\lambda_2}(z)}$. The parameter α also depends slightly on cloud total water content, but since the cloud total water content is a function of the cubic of the cloud drop diameter, small variations in cloud drop diameter produce large variations in total water content, particularly in clouds with large drops. Thus, the parameter α depends primarily on cloud drop size and therefore should be capable of discerning Appendix C from Appendix O conditions. (**b**) The flight data indicates that 120 s mean values of the normalized cloud total water content $T\hat{W}C = \frac{TWC}{\beta}$ depends inversely on 120 s mean values of the *MVD*. Both ice accretion on the OIDU and the dependence of the OIDU measurements on its internal temperature increases the scatter in the data. In the future, we plan a careful calibration of the OIDU in a icing wind tunnel, but this will require the development of an optical system to increased the path length of the laser beams to more than 100 m. The equations describing the models used to generate the dashed curves in this figure are $MVD = \frac{1.740}{\alpha - 0.289}$ and $T\hat{W}C = 0.354e^{-0.004MVD}$, where $\alpha \geq 0.2925$.

in sampling location and volume between the IDS and the reference scientific measurements are expected to be much larger for *TWC* than for *MVD*.

Figure 1 indicates that $\alpha \approx 0.33$ for $MVD \approx 40\,\mu$m, and $\alpha \approx 0.32$ for $MVD \approx 50\,\mu$m. To be conservative and consistent with the definition adopted in the SENS4ICE reports[24], we take $\alpha \leq 0.33$ as the indication of icing conditions of Appendix O. The normalized total water content $T\hat{W}C \equiv \frac{TWC}{\beta}$, where $\beta = \frac{P_{\lambda_3}(z)}{[P_{\lambda_1}(z) - P_{\lambda_2}(z)]}$ is expected to be a function of *MVD*[49], and flight data suggest that this dependence is an exponential function, that is $T\hat{W}C = 0.354e^{-0.004MVD}$ as indicated in Fig. 1b. Both ice accretion on the OIDU and the sensitivity of the OIDU measurements to its internal temperature are likely responsible for some of the scatter in the data. In the future, we plan to calibrate the OIDU in a icing wind tunnel, but this will require the development of an apparatus to increase the path length of the laser beams inside the icing wind tunnel cloud to more than 100 m.

Once the value of *MVD* of a data point is estimated based on $\alpha \equiv \frac{P_{\lambda_3}(z)}{P_{\lambda_2}(z)}$ calculated from measurements of $P_{\lambda_2}(z)$ and $P_{\lambda_3}(z)$, the total water content (*TWC*) at the same data point can be estimated using the relationship between *MVD* and the normalized total water content $T\hat{W}C = \frac{TWC}{\beta}$. We choose to estimate *TWC* instead of *LWC* because: (i) mixed thermodynamic phase icing conditions are more common than pure liquid water icing conditions[52,53]; (ii) the optical effects of liquid water usually dominate the signal under mixed phase conditions, making the separation of the two signals difficult; and (iii) it is prudent to be conservative and err in the direction of overestimating the cloud water content rather than underestimating it.

IDS tests and validation

An IDS conceptual prototype was fabricated and tested before flight units were developed. Details of the MRU and OIDU conceptual prototypes and the IDS flight unit design, as well as results of simulations, tests, and calibrations, are shown in the supplementary information. The complete IDS consists of the MRU, the OIDU, and the IDS controller (IDSC). The IDSC processes the data from MRU and OID measurements, controls the MRU, controls the OIDU, receives power from the aircraft, and interfaces data with the aircraft. Candidate microstrip resonator designs were first tested through numerical simulations with Sonnet®, a commercial software package for high-radio frequency (RF) and microwave electromagnetic analysis. Once the design of the microstrip resonator was selected, the microstrips were fabricated and tested in the laboratory using a network analyzer to excite the resonances through a microwave signal transmitted through port 1 and characterize the resonances through the signal received at port 2, that is the ($|S_{21}|^2$) scatter parameter[38]. This analysis indicates that the MRU is capable of detecting ice accretion layers thinner than 0.3 mm, the threshold required to determine the onset of ice accretion[11]. MRU flight units were then manufactured and tested in the laboratory according to the standard of the Technical Commission's Environmental Conditions and Test Procedures for Airborne Equipment (DO-160)[30] items required by Embraer before integration into the Phenom 300. Some of the DO-160 requirements were verified by analysis or simulations instead of tests.

The conceptual OIDU prototype was developed as a two-band lidar system manufactured using commercial-off-the-shelf parts. Ground tests indicated that the conceptual OIDU was able to infer the thermodynamic phase of cloud water and was sensitive to the size of cloud drops and ice particles. After tests on the ground and in a light aircraft, a third band was added to the OIDU to measure the size of the cloud drops and the cloud water content using an innovative method developed to infer the size and liquid water content of the drizzle[49]. In addition, one of the measurement bands used in the conceptual design was modified to mitigate the effects of absorption by atmospheric water vapor. OIDU flight units were then manufactured and tested in the laboratory under the DO-160 conditions required by Embraer. Some of the DO-160 requirements were met by analysis or simulations.

Flight tests results

Conditions were classified as icing conditions in the SENS4ICE flight campaigns when the $LWC > 0.025$ g/m^3 and the ambient air temperature $T < 0^{\circ}$C[54]. Conditions were classified as Appendix O icing conditions when in addition to these two conditions, more than 1% of the *LWC* was in SLDs, $LWC/TWC > 0.4$, the SLD number concentration $> 100\,\mathrm{m}^{-3}$, the ice crystal number concentration $< 1000\,\mathrm{m}^{-3}$, and the SLD number concentration > 10 times the ice crystals number density[54,55].

Figure 2a shows the values of the parameter α for all flight segments, with values for the Appendix C conditions colored green and values for the more hazardous Appendix O conditions colored red[24]. These results indicated that the parameter α discriminates between the conditions of Appendix C and Appendix O seconds after the aircraft enters each cloud. The reason for this is that α depends primarily on the size of the cloud drops, particularly for $MVD > 40\ \mu$m[49], and that a few measurements are enough to reliably detect icing conditions.

Figure 2b shows the value of the parameter γ for all flight intervals the Phenom 300 encountered icing conditions[24], with Appendix C conditions colored green and the more hazardous Appendix O conditions colored red. Since, for the liquid water phase $\gamma > 0.82$, and for the mixed thermodynamic phase $0.76 < \gamma < 0.82$, the OIDU flight data indicates that liquid water or mixed thermodynamic phase existed in all flight segments in which icing conditions were encountered.

Table 2 summarizes the results of the measurements with the reference scientific measurements, the MRU, and the OIDU during all flights. Except for *MVD* that median values in each flight interval are presented in this table while mean values are presented in Table 1, all other values presented are mean values for each flight interval while the values shown in brackets are standard deviations of the measurements and the parameters estimated to give an idea of their spatial heterogeneity in each flight interval. Considering the variability and uncertainties of the measurements (recall that the errors in the measurements of *MVD* are about ± 20%, and in the measurements of *TWC* they are about ± 40%), the agreement of the measured and estimated values is quite reasonable. The only discrepancies between observations and MRU measurements of ice accretion are in Flight 1479 - Int 1 and in Flight 1482 - Int 1. In Flight 1479 - Int 1, no ice accretion is indicated in the flight log and the MRU indicated ice accretion, but it is likely that there was some accretion on the MRU because the airplane was

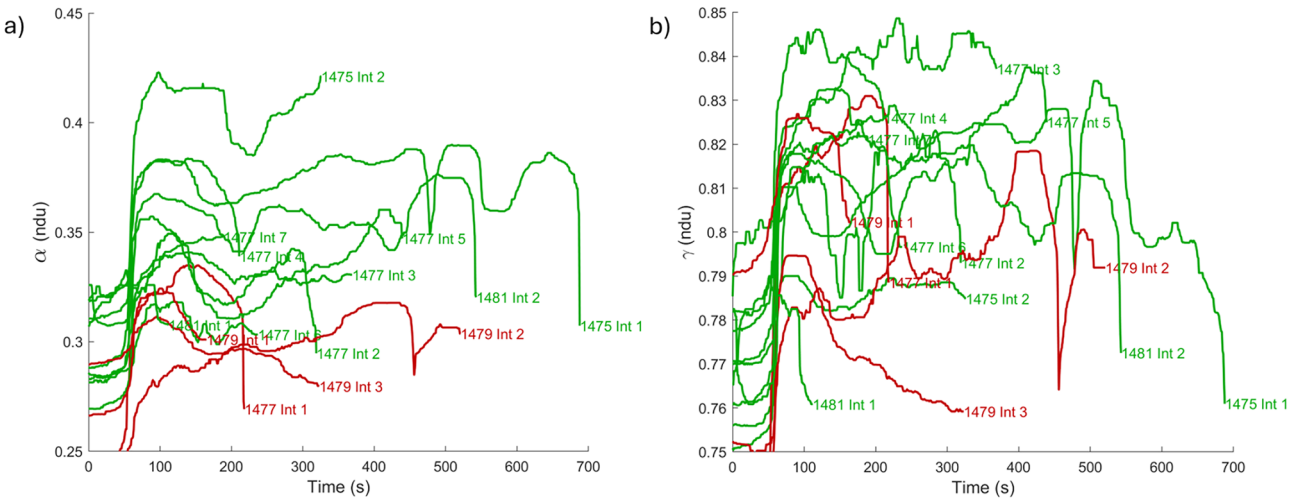

Fig. 2. (**a**) The flight data indicates that the parameter $\alpha \equiv \frac{P_{\lambda_3}(z)}{P_{\lambda_2}(z)}$ is smaller for the flight segments in Appendix O icing conditions than the ones in Appendix C icing conditions, indicating that α alone can be used to determine when an aircraft is flying in the more hazardous Appendix O icing conditions. The OIDU appears to have been colder in Flight 1477 - Int 1, and Flight 1479 - Int 1, which increases α and might explain some of the overlap between Appendix C and O icing conditions. (**b**) The flight data indicates that the parameter $\gamma = \frac{P_{\lambda_2}(z)}{P_{\lambda_1}(z)} > 0.76$ for all flight segments in icing conditions, indicating the Phenom 300 was flying in either liquid water or mixing thermodynamic phase conditions during all icing encounters. The time reference used in this figure is 60 s before the aircraft enters icing conditions according to the SENSE4ICE flight campaign reports[24,51].

Flight #	App.	MVD (μm)	TWC (g/m^3)	LWC/TWC	α	β	γ	MVD (μm)	TWC (g/m^3)	Ice Accr.	f_3/f_d
1475 - Int 1	C	17	0.64	0.88	0.38	1.65	0.81	19	0.54	**Yes**	0.9764
		(1)	(0.11)					(13)	(0.08)	cold	$\pm$0.001
1475 - Int 2	C	15	0.76	0.88	0.41	1.52	0.79	14	0.51	**Yes**	0.966
		(1)	(0.16)					(3)	(0.04)	cold	$\pm$0.004
1477 - Int 1	O	23	0.79	0.72	0.32	1.53	0.82	47	0.44	**Yes**	0.877
		(163)	(0.13)					(95)	(0.11)	cold	$\pm$0.098
1477 - Int 2	C	16	0.41	0.80	0.33	1.55	0.82	37	0.47	**Yes**	0.9679
		(91)	(0.08)					(65)	(0.8)	cold	$\pm$0.002
1477 - Int 3	C	14	0.33	0.90	0.33	1.75	0.84	42	0.52	**Yes**	0.9755
		(95)	(0.08)					(36)	(0.09)	cold	$\pm$0.000
1477 - Int 4	C	17	0.78	0.85	0.38	2.01	0.84	19	0.66	**Yes**	0.9670
		(1)	(0.12)					(3)	(0.06)	cold	$\pm$0.0085
1477 - Int 5	C	17	0.35	0.86	0.33	1.58	0.82	41	0.47	**Yes**	1.0732
		(127)	(0.21)					(54)	(0.12)	hot	$\pm$0.002
1477 - Int 6	C	12	0.11	0.91	0.31	1.35	0.81	85	0.31	**Yes**	0.9916
		(13)	(0.09)					(191)	(0.18)	cold	$\pm$0.001
1477 - Int 7	C	17	0.34	0.88	0.34	1.56	0.82	32	0.49	**Yes**	0.9783
		(51)	(0.12)					(10)	(0.07)	hot	$\pm$0.001
1479 - Int 1	O	23	0.23	0.77	0.32	1.49	0.82	65	0.39	No	0.9774
		(131)	(0.13)					(85)	(0.12)	cold	$\pm$0.000
1479 - Int 2	O	185	0.24	0.88	0.30	1.18	0.79	170	0.21	**Yes**	0.9538
		(52)	(0.15)					(195)	(0.13)	cold	$\pm$0.022
1479 - Int 3	O	23	0.02	0.99	0.30	1.03	0.77	247	0.16	**Yes**	0.9698
		(71)	(0.05)					(194)	(0.11)	cold	$\pm$0.002
1481 - Int 1	C	20	0.17	0.88	0.33	1.19	0.78	40	0.34	–	0.9774
		(8)	(0.15)					(56)	(0.10)		$\pm$0.000
1481 - Int 2	C	22	0.48	0.88	0.36	1.52	0.81	25	0.49	–	0.9774
		(12)	(0.20)					(9)	(0.07)		$\pm$0.000
1482 - Int 1	C	14	0.51	0.94	0.36	–	–	–	–	Yes	0.9765
		(2)	(0.21)							cold	$\pm$0.001
1482 - Int 2	C	14	0.50	0.95	0.36	–	–	–	–	**Yes**	0.9765
		(1)	(0.23)							cold	$\pm$0.001

Table 2. Summary of the Phenom 300 data for flight intervals (Int) in which the IDS was turned on showing parameters measured by the reference scientific instruments, logbook notes indicating ice accretion or not in the column titled Ice Accr., predicted values of MVD and TWC in bold, and results of MRU measurements $\mathbf{f_3/f_d}$ also in bold indicating ice accretion ($f_3/f_d < 0.98$) or not ($f_3/f_d \geq 0.98$). Except for MVD that median values are presented for each entire flight interval, all other values are mean for the flight interval, while the values in brackets are standard deviations. Yes under Ice Accr. indicates that ice accretion was observed to occur in the flight interval, while No indicates that that ice accretion was not observed to occur. **Yes** in bold indicates that in addition to the observation of ice accretion in the flight interval, observations just before the airplane entered the flight interval are consistent with the MRU measurements at the start of the flight interval (indicating ice accreted or not) and its phase in the heating cycle. Indeed, the 'cold' and 'hot' remarks indicates whether the MRU was in a cooling (allowing ice accretion), or a heating (preventing ice accretion) phase of the cycle designed to shed ice from it (periodically), at the start of the flight interval. The ice accretion observations are from notes in the flight log[51] and therefore are qualitative. Since the OIDU temperature was well below its calibrated range in flight 1482, the results for this flight interval are not reliable and therefore are not shown.

flying in freezing drizzle. In Flight 1482 - Int 1 there is no indication of ice accretion in the flight log, but this flight interval was just after takeoff; some ice might have formed on the MRU as the airplane was moved from the warm and humid hangar to outside. Since usually *MVD* and *TWC* vary significantly in most flight internals, the sampling volume of the reference scientific measurements and of the OIDU differ by many orders of magnitude, their measurements are more than 50 m apart, and the measurement errors are significant as indicated by the standard deviations, the agreement between measured and predicted values is good. In the future, we plan to conduct more controlled laboratory measurements to further assess the performance of the OIDU.

Figure 3 shows Phenom 300 reference scientific measurements and IDS measurements of all quantities of interest measured by the reference instruments and the OIDU in two flight intervals in which the Phenom 300 encountered the prevailing Appendix C icing conditions and in two flight intervals in which it encountered the more hazardous Appendix O icing conditions. The predicted 60 s running mean values of *MVD* and *TWC* agree within a factor of about 2 with the values measured by the reference instruments, when taking into account the uncertainties in the measurements. On Flight 1479 Interval 3, the predicted *MVD* value is off-scale. A problem with the comparison is the mismatch in sampling volume between the reference instruments and the OIDU discussed previously. The values of *MVD* measured by the reference instruments have large variations in the flight segments in the conditions of Appendix O, suggesting that spatial variations should also be expected. This complicates the comparison of the OIDU measurements with those of the reference instruments. However, since the primary goal of the IDS is to distinguish the icing conditions of Appendix C from the conditions of Appendix O, and this can be done through the parameter α as illustrated in Fig. 2, estimating the physical cloud parameters is less important.

Measurements of ice accretion by MRU are shown in Fig. 4. Only the center frequency $f_{i=3}$ of the resonance mode $i = 3$ is shown in the MRU measurements because a low signal-to-noise ratio prevented the calculation of the quality factor Q_3 reliably, as shown in the supplementary information. The MRU RF circuit needs to be improved to mitigate internal interference noises. The MRU microstrip sensor was heated every 4 minutes from flight # 1475 to 1477 to shed ice formed on it, and this heating cycle was increased to 8 minutes afterward. Laboratory measurements indicate $f_{i=3} = 2.6525 \pm 0.015$ GHz, and simulations indicate that a 0.3 mm thick layer of pure ice reduces this resonance frequency by 0.075 GHz. Thus, conservatively, we take $f_3/f_d < 0.98$ as an indication of ice accretion.

The IDS measurements indicate that the OIDU detects icing conditions seconds after the aircraft enters the cloud, while the MRU detects ice accretion (indicated by a decrease in the resonance frequency) also shortly

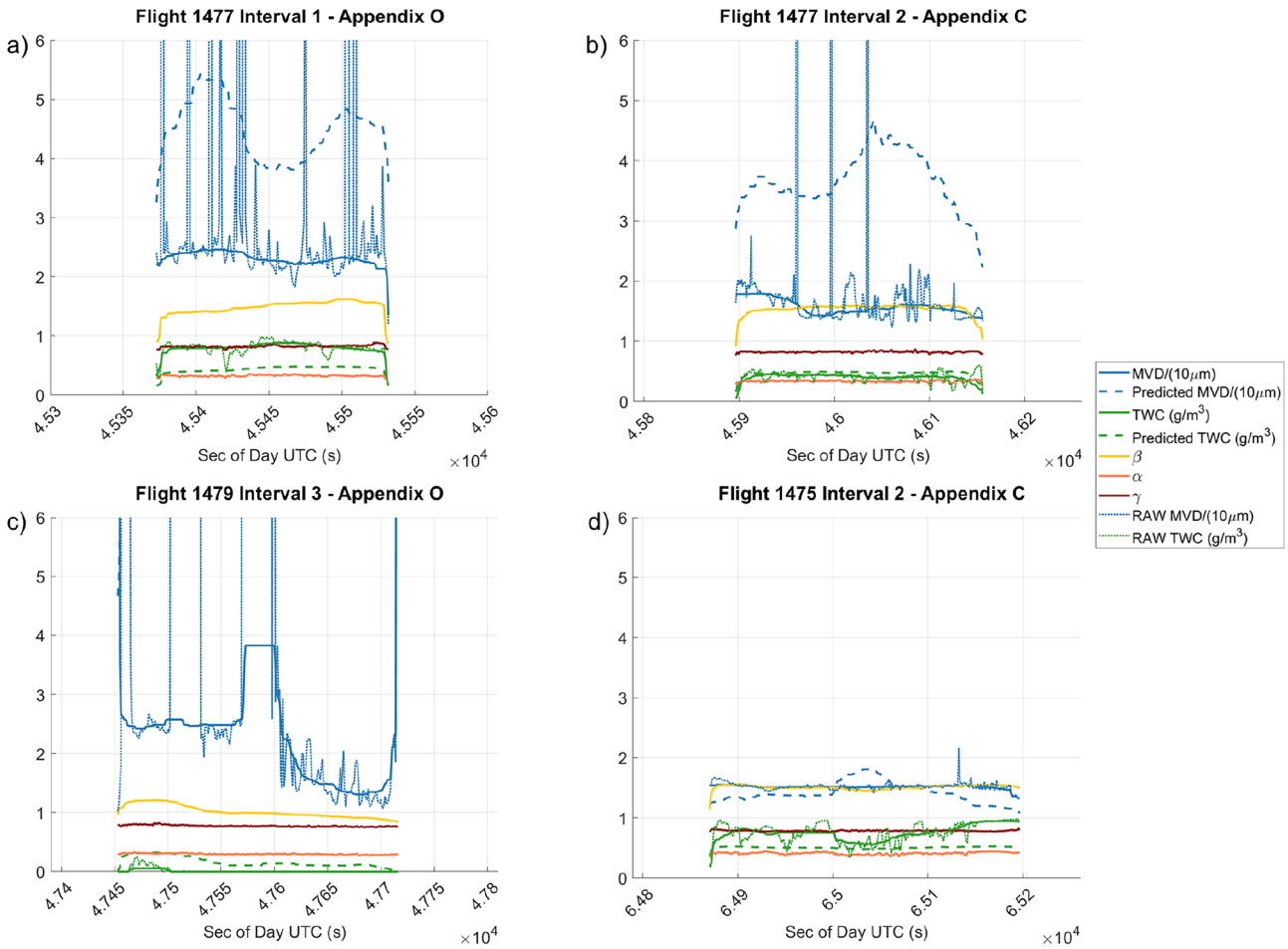

Fig. 3. Reference scientific measurements and OIDU measurements for two flight intervals in which the Phenom 300 encountered prevailing Appendix O icing conditions (Flight 1477 Interval 1, and Flight 1479 Interval 3) and for two flight intervals in which it encountered the less hazardous Appendix C icing conditions (Flight 1477 Interval 2, and Flight 1475 Interval 2). The vertical axis represents the normalized values described in the insert on the right. Time is given in seconds of the day in Greenwich (UTC) for comparison with the SENSE4ICE flight campaign reports[24,51]. The measurements indicate that, in both Appendix O and Appendix C conditions, the OIDU detects icing seconds after the aircraft enters the cloud.

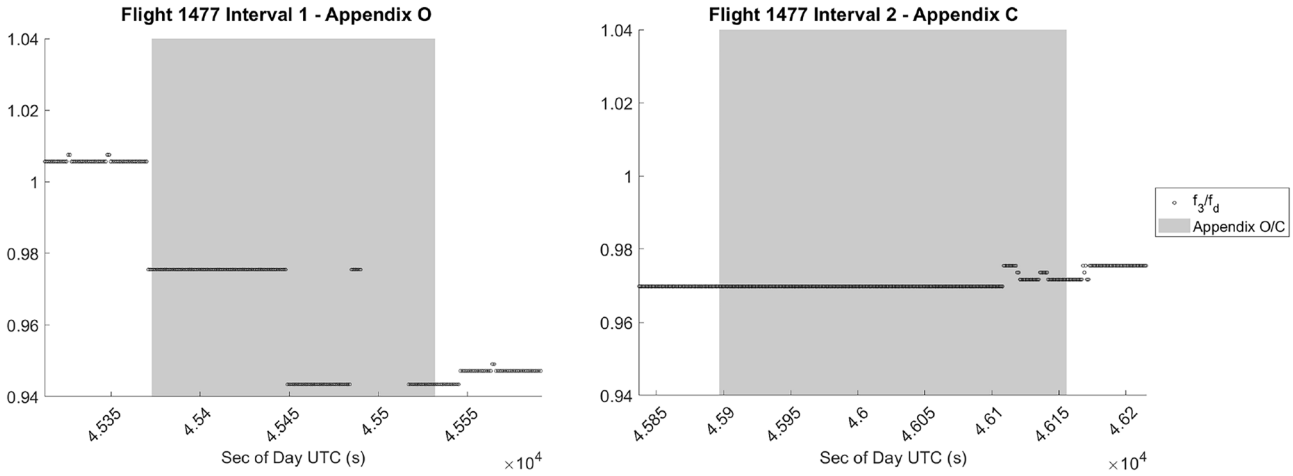

Fig. 4. MRU measurements for a flight interval in which the Phenom 300 encountered prevailing Appendix O (Flight 1477 Interval 1) and for a flight interval in which it encountered the less hazardous Appendix C (Flight 1477 Interval 2) icing conditions. Time is given in seconds of the day in Greenwich (UTC) for comparison with the SENSE4ICE flight campaign reports[24,51]. The MRU detects ice accretion conditions seconds after the aircraft enters Appendix O icing conditions indicated by an abrupt decrease in the resonance frequency. These flight intervals were selected because in the Flight 1475 Interval 2 and in Flight 1479 Interval 3 the MRU sensing unit had ice accreted in previous flight segments while approaching the icing conditions, and significant ice accretion did not occur in these flight segments. The heater of the MRU sensing unit was cycled continuously during flight to prevent substantial ice accretion.

after the aircraft enters Appendix O conditions. Since ice accretion was not measured independently near the MRU, reference measurements are not available for comparison. The MRU center resonance frequency is normalized to 2.65 GHz, the approximate value (slightly smaller than it) of the center resonance frequency with the dry microstrip resonator. In Flight 1477 Interval 2, a small amount of ice accreted in the previous flight segment appears to be accreted on the microstrip while the aircraft was approaching the cloud, and no further ice accretion occurs. This flight data indicates that the IDS is capable of detecting ice accretion onto the aircraft and of discriminating between Appendix C and Appendix O icing conditions. As summarized in Tables 1 and 2 the IDS performed well in all other flights under icing conditions.

Discussion

Ice accretion by the impact of water drops below 0°C, referred to as supercooled water drops, or mixtures of these drops and ice particles, referred to as mixed phase, on an aircraft in flight is a hazard, referred to as aircraft icing. Large water drops are more dangerous than smaller drops because they can cause ice accretion in areas of the aircraft that are not protected by the deicing system. Typical General Aviation (GA) aircraft icing detection procedures consist simply of a notification to the pilot that the air temperature is below about 0°C. Unfortunately, temperature alone is not enough to infer the occurrence of icing because it requires the presence of supercooled water drops in the atmosphere around the aircraft.

Aircraft certified to fly into icing conditions, like commercial transport airplanes, currently have simplistic icing detection probes mounted on the airplane's nose cone, while ice accretion in the airplane wings and horizontal stabilizer is what usually results in hazardous flight conditions. More stringent Aircraft Certification Specifications (ACS) were recently developed in response to the discovery that ice accretion caused by the impact of supercooled large droplets (SLD) has caused several catastrophic aircraft accidents in the past few decades. Compliance with these ACS requires new types of icing detection systems capable of discriminating between common icing conditions and more hazardous SLD icing conditions that cause ice accretion on unprotected aircraft surfaces. These new icing detection systems are required to measure both ice accretion onto the aircraft and the icing-hazard potential of the atmosphere around the aircraft.

The results of flight tests of our new icing detection system (IDS) in a jet aircraft, with scientific instruments for reference measurements, indicate that it is capable of detecting ice accretion onto the aircraft and discriminating between common icing conditions and the more hazardous SLD icing conditions in the atmosphere surrounding the aircraft. In addition, the IDS is capable of inferring the size of the cloud drop and the total water content to further assess the level of icing hazard. The IDS prototype needs to mature further and then be certified, but the results of flight tests reported here indicate that it is a robust instrument capable of contributing to increases in flight safety. Some of the challenges that still need to be addressed are the installation of a heater on the OIDU to control its internal temperature to prevent signal drifts, the reduction of radio frequency (RF) noise in the MRU to improve its performance, and in particular to allow the determination of the type of ice accreted, the ice thickness, and the thickness of water films to allow the estimation of the cloud liquid water content, in addition to total water content. The IDS will then be ready to be fully tested in an icing wind tunnel and certified.

Data availability

The flight test data are available at the University of Michigan's Deep Blue Data repository.

Received: 23 October 2024; Accepted: 25 November 2025
Published online: 26 January 2026

References

1. Petty, K. R. & Floyd, C. D. J. A statistical review of aviation airframe icing accidents in the us. In *Proc. of the 11th Conference on Aviation, Range, and Aerospace Hyannis* (2004).
2. Appiah-Kubi, P. Us inflight icing accidents and incidents, 2006 to 2010 (2011).
3. Jones, S. M., Reveley, M. S., Evans, J. K. & Barrientos, F. A. *Subsonic aircraft safety icing study* (Tech. Rep. NASA, 2008).
4. NTSB. In-flight icing encounter and loss of control; simmons airlines, American eagle flight 4184; Roselawn, Indiana; October 31, 1994. Tech. Rep., NTSB (1996).
5. Cao, Y., Tan, W. & Wu, Z. Aircraft icing: An ongoing threat to aviation safety. *Aerosp. Sci. Technol.* **75**, 353–385 (2018).
6. de Investigação e Prevenção de Acidentes Aeronáuticos (CENIPA), C. Perda de controle - foramacao de gelo - 9/agosto/2024 (2024).
7. Jackson, D. G. & Goldberg, J. I. Ice detection systems: A historical perspective. *SAE Technical Paper* (2007).
8. Jeck, R. K. *A history and interpretation of aircraft icing intensity definitions and faa rules for operating in icing conditions* (Tech. Rep. Citeseer, 2001).
9. Leopold, D. Flight in icing regulatory evolution and the influence on aircraft design. *SAE Int. J. Adv. Curr. Pract. Mobil.* **2**, 71–77 (2019).
10. Jackson, D. G. Primary ice detection certification under the new faa and easa regulations. *SAE Technical Paper* (2015).
11. SAE. Minimum operational performance specification for inflight icing detection systems (2022).
12. Richard, J. D. Ice detection apparatus (1966).
13. Otto, J. T. *et al.* Ice detector for improved ice detection at near freezing condition (2006).
14. Fraser, D. *Meteorological Design Requirements for Icing Protection Systems* (National Aeronautical Establishment Canada, 1953).
15. Fraser, D., Rush, C. & Baxter, D. Thermodynamic limitations of ice accretion instruments. *Bull. Am. Meteor. Soc.* **34**, 146–154 (1953).
16. Lozowski, E. *et al.* Spongy icing revisited: Measurements of ice accretion liquid fraction in two icing tunnels. In *43rd AIAA Aerospace Sciences Meeting and Exhibit*, 658 (2005).
17. Renno, N. O. Aircraft icing detector (2016).
18. Renno, N. O. Ice and supercooled water detection system (2016).
19. Renno, N. O. Ice and water detection system (2016).
20. Ray, M. & Anderson, K. Analysis of flight test results of the optical ice detector. *SAE Int. J. Aerosp.* **8**, 1–8 (2015).
21. Anderson, K. J. & Ray, M. D. *Sld and ice crystal discrimination with the optical ice detector* (SAE Technical Paper, 2019).
22. Halama, G., Ray, M., Anderson, K., Nesnidal, M. & Ide, R. Optical ice detection: Test results from the nasa glenn icing research tunnel. In *AIAA Atmospheric and Space Environments Conference*, 7532 (2010).
23. Schwarz, C. W. The sens4ice eu project–sensors and certifiable hybrid architectures for safer aviation in icing environment–project overview and initial results. *Proc. of the International Council of the Aeronautical Sciences (ICAS), Stockholm, Sweden*, 4–9 (2022).
24. Deiler, C. Performance-based ice detection-first results from sens4ice European flight test campaign. In *AIAA SciTech 2024 Forum*, 2817 (2024).
25. Roberts, I., Gent, R., Hatch, C. & Moser, R. *Development of the atmospheric icing patch (aip) under the sens4ice programme* (SAE Technical Paper, 2023).
26. Hamman, M. et al. *Development and validation testing of the collins ice differentiator system in app c and app o icing conditions* (SAE Technical Paper, 2023).
27. Pohl, M. Flight testing a lamb wave based ice accretion sensor. *In AIAA Aviation Forum and Ascend* **2024**, 3525 (2024).
28. González, M. & Frövel, M. Fiber Bragg grating sensors ice detection: Methodologies and performance. *Sens. Actuat. A* **346**, 113778 (2022).
29. del Val, M. G. & Frövel, M. Flight tests results of a fiber Bragg gratings based ice sensor. *Cold Reg. Sci. Technol.* **224**, 104248 (2024).
30. Borgstrom, E. J. An overview of the emc requirements in rtca/do-160d. In *1998 IEEE EMC Symposium. International Symposium on Electromagnetic Compatibility. Symposium Record (Cat. No. 98CH36253)*, vol. 2, 702–707 (IEEE, 1998).
31. Kendra, J. R., Ulaby, F. T. & Sarabandi, K. Snow probe for in situ determination of wetness and density. *IEEE Trans. Geosci. Remote Sens.* **32**, 1152–1159 (1994).
32. Sarabandi, K. & Li, E. S. Microstrip ring resonator for soil moisture measurements. *IEEE Trans. Geosci. Remote Sens.* **35**, 1223–1231 (1997).
33. Mazzaro, G. J. In-situ permittivity measurements using ring resonators. In *Radar Sens. Technol. XVI* Vol. 8361 332–345 (SPIE, 2012).
34. Chen, L.-F., Ong, C. K., Neo, C., Varadan, V. V. & Varadan, V. K. *Microwave Electronics: Measurement and Materials Characterization* (Wiley, 2004).
35. Fratticcioli, E., Dionigi, M. & Sorrentino, R. A simple and low-cost measurement system for the complex permittivity characterization of materials. *IEEE Trans. Instrum. Meas.* **53**, 1071–1077 (2004).
36. Rennó, N. et al. A simple instrument suite for characterizing habitability and weathering: The modern aqueous habitat reconnaissance suite (mahrs). *Astrobiology* **19**, 849–866 (2019).
37. Jiang, J. H. & Wu, D. L. Ice and water permittivities for millimeter and sub-millimeter remote sensing applications. *Atmos. Sci. Lett.* **5**, 146–151 (2004).
38. Guillon, P. & Kajfez, D. *Dielectric Resonators* (Noble Publishing, 1998).
39. Petersan, P. J. & Anlage, S. M. Measurement of resonant frequency and quality factor of microwave resonators: Comparison of methods. *J. Appl. Phys.* **84**, 3392–3402 (1998).
40. Twomey, S. & Seton, K. Inferences of gross microphysical properties of clouds from spectral reflectance measurements. *J. Atmos. Sci.* **37**, 1065–1069 (1980).
41. Nakajima, T. & King, M. D. Determination of the optical thickness and effective particle radius of clouds from reflected solar radiation measurements. part i: Theory. *J. Atmos. Sci.* **47**, 1878–1893 (1990).
42. Pilewskie, P. & Twomey, S. Cloud phase discrimination by reflectance measurements near 1.6 and 2.2 μm. *J. Atmos. Sci.* **44**, 3419–3420 (1987).
43. Pilewskie, P. & Twomey, S. Discrimination of ice from water in clouds by optical remote sensing. *Atmos. Res.* **21**, 113–122 (1987).
44. Kokhanovsky, A. A. *Cloud Optics* Vol. 283 (Springer, 2006).
45. Ehrlich, A. et al. Cloud phase identification of arctic boundary-layer clouds from airborne spectral reflection measurements: test of three approaches. *Atmos. Chem. Phys.* **8**, 7493–7505 (2008).
46. Martins, J. V. et al. Remote sensing the vertical profile of cloud droplet effective radius, thermodynamic phase, and temperature. *Atmos. Chem. Phys.* **11**, 9485–9501 (2011).

47. Rennó, N. O. et al. Chaser: An innovative satellite mission concept to measure the effects of aerosols on clouds and climate. *Bull. Am. Meteor. Soc.* **94**, 685–694 (2013).
48. Thompson, D. R. et al. Measuring cloud thermodynamic phase with shortwave infrared imaging spectroscopy. *J. Geophys. Res. Atmos.* **121**, 9174–9190 (2016).
49. Westbrook, C., Hogan, R., O'Connor, E. & Illingworth, A. Estimating drizzle drop size and precipitation rate using two-colour lidar measurements. *Atmos. Meas. Tech.* **3**, 671–681 (2010).
50. Kou, L., Labrie, D. & Chylek, P. Refractive indices of water and ice in the 0.65-to 2.5-μm spectral range. *Appl. Opt.* **32**, 3531–3540 (1993).
51. Embraer. Sld natural ice campaign test results. Tech. Rep., Embraer (2023).
52. Sand, W. R., Cooper, W. A., Politovich, M. K. & Veal, D. L. Icing conditions encountered by a research aircraft. *J. Appl. Meteorol. Climatol.* **23**, 1427–1440 (1984).
53. Heggli, M. F., Vardiman, L., Stewart, R. E. & Huggins, A. Supercooled liquid water and ice crystal distributions within Sierra Nevada winter storms. *J. Clim. Appl. Meteorol.* **1**, 1875–1886 (1983).
54. Lucke, J., Zollo, A., Bernstein, B. & Jurkat-Witschas, T. Sens4ice deliverable d4. 3: final report on airborne demonstration and atmospheric characterization. Tech. Rep., Technical report, Deutsches Zentrum für Luft-und Raumfahrt eV (2024).
55. Cober, S. G. & Isaac, G. A. Characterization of aircraft icing environments with supercooled large drops for application to commercial aircraft certification. *J. Appl. Meteorol. Climatol.* **51**, 265–284 (2012).

Acknowledgements

We would like to thank the National Science Foundation for supporting the development of the Microwave Resonator Unit (MRU) and its integration with the Optical Icing Detection Unit (OIDU) to complete the Icing Detection System (IDS) under PFI-TT Award Number 2044245, and Embraer for inviting us to test the IDS in the Phenom 300 flight campaign.

Author contributions

Nilton O. Renno conceived the icing detection system (IDS), led the data analysis, and wrote the article; Roger Backhus designed the MRU electronics, conducted numerical simulations of the microstrip resonator, and supported laboratory tests and calibrations of the MRU; Timothy Butler developed the MRU firmware, and supported laboratory tests and calibrations of the MRU; Curt Cooper developed the OIDU electronics, and supported laboratory tests and calibrations of the OIDU; Kurt A. Hochrein supported tests of the conceptual OIDU prototype; Rohan Madathil supported the analysis of the flight test data; Louis Marr designed the IDS mechanical subsystems, and conducted dynamics simulations of the IDS; Ryan Miller developed the OIDU FPGA firmware; Paul Mohan managed the OIDU system engineering activities and OIDU measurement calibration procedures; Stephen Musko developed the IDS data communication protocol, the IDS controller, procedures for interfacing with the aircraft, and overall IDS software, and led the IDS qualification tests; Thomas Ryan designed the OIDU optics and supported the development of the OIDU calibration and test procedures; Fernando Saca led the MRU system engineering efforts and supported laboratory tests and calibrations of the MRU; and Jeffrey Zewicke developed the conceptual OIDU prototype and supported its calibrations and tests. All authors reviewed the manuscript.

Declarations

Competing interests

Nilton O. Renno and Kurt A. Hochrein declare they have personal financial interests in the New Aircraft Icing Detection System (IDS) by owning shares of Intelligent Vision Systems (IVS).

Additional information

Supplementary Information The online version contains supplementary material available at https://doi.org/10.1038/s41598-025-30681-3.

Correspondence and requests for materials should be addressed to N.O.R.

Reprints and permissions information is available at www.nature.com/reprints.

Publisher's note Springer Nature remains neutral with regard to jurisdictional claims in published maps and institutional affiliations.